



Geophysical Research Letters

RESEARCH LETTER

10.1029/2020GL088057

Key Points:

- Non-additivity is found in the circulation response to regional Arctic temperature anomalies
- Stratosphere-troposphere coupling contributes to the non-additivity
- Non-additivity also generally increases with forcing amplitude

Supporting Information:

- Supporting Information S1

Correspondence to:

B. De,
bd2529@columbia.edu

Citation:

De, B., Wu, Y., & Polvani, L. M. (2020). Non-additivity of the midlatitude circulation response to regional Arctic temperature anomalies: The role of the stratosphere. *Geophysical Research Letters*, 47, e2020GL088057. <https://doi.org/10.1029/2020GL088057>

Received 27 MAR 2020

Accepted 1 AUG 2020

Accepted article online 10 AUG 2020

Non-Additivity of the Midlatitude Circulation Response to Regional Arctic Temperature Anomalies: The Role of the Stratosphere

Bitih De^{1,2,3} , Yutian Wu² , and Lorenzo M. Polvani^{2,3} 

¹Department of Earth, Atmospheric and Planetary Sciences, Purdue University, West Lafayette, IN, USA, ²Lamont-Doherty Earth Observatory, Columbia University, Palisades, NY, USA, ³Department of Applied Physics and Applied Mathematics, Columbia University, New York, NY, USA

Abstract Previous studies have documented the impact of the Arctic sea ice loss and associated warming on the midlatitude weather and climate, especially the influence of sea ice retreat over the Barents-Kara Sea on the North Atlantic and Europe regions. However, less attention has been given to other geographical locations over the Arctic, and to the linear additivity of the circulation response to regional Arctic sea ice loss and temperature anomalies. Using a simplified dry dynamical core model, we demonstrate that responses to regional Arctic temperature anomalies over the Barents-Kara Sea, Baffin Bay-Davis Strait-Labrador Sea, and East Siberia-Chukchi Sea, separately, cause similar equatorward shift of the tropospheric jet, but different stratospheric polar vortex responses. Furthermore, responses to regional Arctic temperature anomalies are not linearly additive, and the residual resembles a positive Northern Annular Mode-like structure. Additional targeted experiments highlight the stratospheric influence in the non-additivity of the midlatitude tropospheric response.

Plain Language Summary One of the primary consequences of the rapid melting of the Arctic sea ice, concurrent with the rising CO₂, is an amplified warming over the Arctic than the rest of the globe. At the same time, its possible linkage to cold extremes across the midlatitude continents has attracted much scientific and socioeconomic attention. However, discrepancies are found in previous modeling studies on the role of the Arctic sea ice loss and associated warming. Our results suggest that some of the discrepancies could be due to the differences in the forcing as the responses are sensitive to the forcing location and sum of the responses to individual regional forcing overestimates the response to simultaneous forcing. Therefore, we caution that results from regional sea ice loss might not provide the correct picture of pan-Arctic sea ice melting.

1. Introduction

Unprecedented sea ice loss and amplified warming over the Arctic (known as the Arctic amplification, or AA) has been observed in the recent decades (e.g., Screen & Simmonds, 2010). Previous observational and modeling studies have suggested a potential influence of the Arctic sea ice loss on the midlatitude circulation during Northern Hemisphere (NH) winter (see review papers by Barnes & Screen, 2015; Cohen et al., 2014, and references therein). Nevertheless, how and to what extent the AA contributes to the modulation of the midlatitude circulation remains inconclusive due to discrepancies found in previous studies and incomplete understanding of the underlying mechanisms (Screen et al., 2018).

It has been suggested that the atmospheric circulation response is sensitive to the geographical location and spatial pattern of the Arctic sea ice loss (McKenna et al., 2018; Screen, 2017; Screen et al., 2018; Sun et al., 2015; Zhang et al., 2017). However, the bulk of previous work focused on the impacts of the sea ice melting over either the pan-Arctic (McCusker et al., 2016; Ogawa et al., 2018; Screen et al., 2015; Sun et al., 2016) or the Barents-Kara Sea (BKS) (De & Wu, 2018; Kim et al., 2014; Mori et al., 2014; Zhang et al., 2018). Circulation responses including a weakening of the stratospheric polar vortex and an equatorward shift of the midlatitude jet were commonly found. Only a few studies highlighted the opposing impacts on the stratospheric polar vortex associated with the sea ice loss over different Arctic regions (McKenna et al., 2018; Sun et al., 2015). For instance, Sun et al. (2015) found a stratospheric polar vortex weakening with sea ice loss

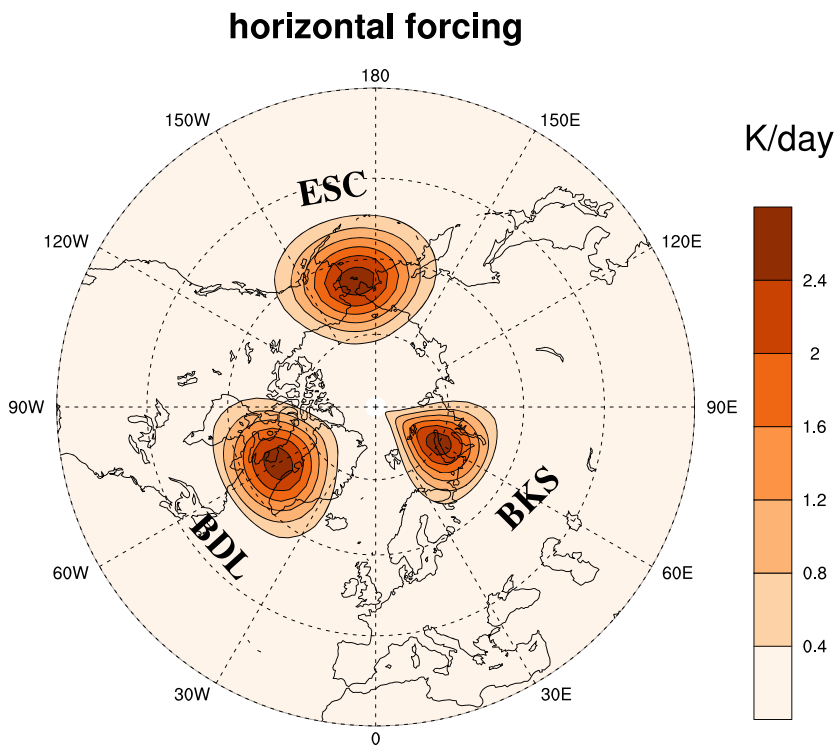


Figure 1. Spatial structure of the prescribed heating rate (color shadings and black contours, with contour interval 0.4 K/day) at the lowest model level for $Q_0 = 3.5$ K/day.

inside the Arctic Circle (primarily over the BKS) but a strengthening with sea ice loss outside the Arctic Circle (mainly over the Bering Sea, Sea of Okhotsk, and Hudson Bay).

In a recent study, Screen (2017) divided the whole Arctic into nine sub-regions to contrast the impacts of regional Arctic and pan-Arctic warming, using the comprehensive Atmospheric General Circulation Model (AGCM) HadGEM2. In each of the perturbation experiments, Screen (2017) imposed the sea ice forcing over individual regions by subtracting two standard deviations of monthly sea ice concentration (SIC) from the climatology at each ice-covered grid and adding two standard deviations of monthly sea surface temperature to the climatology over partially ice-covered grids. The study showed that the response to pan-Arctic sea ice loss cannot be obtained by a simple linear addition of the responses to regional sea ice loss. Hence, a nonlinear interaction among the responses to regional sea ice loss was suggested; however, the underlying dynamical mechanism remains unexplained. This motivates us to further investigate the linear additivity problem. We do so here using a simple AGCM. Compared to a comprehensive AGCM, the simple AGCM has the advantage in isolating the dynamics from uncertainties that arise due to complex physical parameterizations in comprehensive atmospheric model, sea ice model, and their coupling. In this way, our simple model serves as a useful testbed for the robustness of the results reported in comprehensive AGCMs. In addition, the computational efficiency of simple AGCM also facilitates the exploration of the sensitivities of the responses to forcing amplitude. Targeted experiments can also be easily implemented to aid the interpretation of the underlying dynamical mechanism.

In this study, as shown in Figure 1, we focus on three regions over the Arctic: BKS, Baffin Bay-Davis Strait-Labrador Sea (BDL), and East Siberia-Chukchi sea (ESC), and the reasons for this choice are the following. In recent decades, the Arctic has warmed up the most over the BKS and BDL regions (see their Figure 2, Shepherd, 2016). Possible influences on Eurasia cooling associated with BKS sea ice loss (Mori et al., 2014; Zhang et al., 2018) and on North America cooling following ESC and BDL sea ice loss (Chen & Luo, 2017; Kug et al., 2015; Overland & Wang, 2018) were suggested in previous studies. Therefore, these three regions are likely to play key roles in affecting the midlatitude circulation and weather extremes.

With simple AGCM experiments, we aim to address the following questions: (1) What are the impacts of the regional Arctic Temperature Anomalies (or ATA), separately and simultaneously, on the stratospheric polar vortex and the tropospheric circulation? (2) Are these responses linearly additive? If not, what is the underlying dynamical mechanism? (3) How do the results vary with forcing amplitude? This paper is organized as follows. In section 2, we describe the methodology and experimental design using the simple AGCM. In section 3, we present the zonal mean zonal wind response to regional ATA and investigate the linear additivity, its underlying mechanism, and sensitivity to forcing amplitude. Section 4 concludes the paper.

2. Data and Methods

2.1. Observations

We analyze monthly SIC data obtained from passive microwave satellite measurements with NASA team algorithm (Cavalieri et al., 1996) during 1982–2015. The monthly atmospheric variables from the ERA Interim reanalysis data produced by the European Center for Medium-Range Weather Forecasts (ECMWF) are used during the same period (Dee & Coauthors, 2011). We define monthly SIC index using detrended and standardized SIC anomaly, area averaged over the BKS (70° – 80° N, 10° – 110° E), BDL (55° – 75° N, 270° – 310° E), and ESC (65° – 82° N, 160° – 210° E) regions, respectively, from November to subsequent February. Each region is highlighted by a black box in Figure S1 in the supporting information. In order to identify the responses in surface air temperature and circulation associated with regional SIC variability, we perform lagged regression analysis between monthly SIC indices and atmospheric variables during boreal winter. Both the long-term trend and contribution from the El Niño-Southern Oscillation (or ENSO, derived as linear regression on Niño 3.4 index) are removed from the atmospheric variables prior to the regression analysis. We also reverse the sign of the SIC indices to emphasize the response associated with SIC loss. Note that we define SIC index for BKS using November SIC and for BDL and ESC using December and January SIC. This is because the concurrent surface warming associated with the SIC loss is maximized in those respective months for each region (not shown).

2.2. Numerical Model

We perform a set of numerical experiments using a dry dynamical core, developed at the Geophysical Fluid Dynamics Laboratory (GFDL). The model integrates the primitive equations driven by idealized physics (Held & Suarez, 1994) and includes a simple representation of the stratospheric polar vortex (Polvani & Kushner, 2002) and a realistic topography to excite stationary waves (Smith et al., 2010). The model has a spectral T42 horizontal resolution and 40 sigma levels in the vertical with a model top at 0.02 hPa. In this study, we use two model configurations: a standard one and a no stratospheric polar vortex one (novortex hereafter). The standard configuration, with a polar vortex and stratospheric-tropospheric coupling, is identical to Wu and Smith (2016) and Zhang et al. (2017). As found previously, this standard model configuration simulates a tropospheric jet located at about 40° N that is close to the observed winter climatology (Wu & Smith, 2016) and a fairly realistic stationary wave climatology (Zhang et al., 2017). In addition to the standard configuration, we also use a no-vortex configuration to examine the role of stratosphere-troposphere coupling. The no-vortex configuration is identical to the standard configuration except that the lapse rate of the radiative equilibrium profile is set to zero in the stratosphere and no topography is imposed. Note that the control climatologies are mostly similar with or without topography in the no-vortex configuration (not shown). To simplify the analysis, we integrate the model under perpetual winter conditions.

2.3. Experimental Design

For each forcing region (ESC, BDL, BKS, and ALL), we perform a perturbation experiment and compare it against a long control (CTRL) integration. In these experiments, we impose an additional heating, ΔQ , to the temperature tendency equation as follows:

$$\frac{\partial T}{\partial t} = \dots - \kappa_T [T - T_{eq}] + \Delta Q, \quad (1)$$

where κ_T is the Newtonian relaxation time scale and is $\frac{1}{40}$ day $^{-1}$ and T_{eq} is the original radiative equilibrium temperature profile and is a function of latitude ϕ and sigma level σ . The imposed heating rate, ΔQ , as a function of longitude λ , latitude ϕ , and sigma level σ , is designed to mimic the structure of the observed temperature anomaly associated with sea ice loss over ESC, BDL and BKS regions.

Figure S1 shows the regressed surface air temperature on SIC index for the three Arctic regions in observations. We choose the zonal and meridional profile of the prescribed heating based on Figure S1. The regressed temperature profile extends to the midtroposphere, with slightly varying altitudes for each region (not shown). For simplicity, the vertical depth of the prescribed heating is chosen to be identical for each region. Accordingly, here are the imposed heating rates:

$$\Delta Q = Q_0 \cos^k \left(\frac{5}{2} (\phi - \phi_0) \right) e^{m(\sigma - 1)} \sin^n \left(\frac{3}{2} \lambda - \lambda_0 \right),$$

for ESC run, $\phi \geq 50^\circ N$, $\phi_0 = 64^\circ N$, $150^\circ < \lambda < 250^\circ E$, $\lambda_0 = 193^\circ E$,
for BDL run, $\phi \geq 55^\circ N$, $\phi_0 = 67^\circ N$, $250^\circ < \lambda < 350^\circ E$, $\lambda_0 = 0$,
for BKS run, $\phi \geq 65^\circ N$, $\phi_0 = 75^\circ N$, $10^\circ < \lambda < 110^\circ E$, $\lambda_0 = 0$,

(2)

where $k = 12$, $m = 5$, $n = 4$ are chosen to mimic the observed heating profile (as shown in Figure S1). The ALL run is conducted with imposed heating over all three regions simultaneously. In sections 3.1 and 3.2, as a primary example, we use a heating rate $Q_0 = 3.5$ K/day. The horizontal structure of the prescribed heating profile is shown in Figure 1, and the corresponding vertical profile is shown in Figure S2 for $Q_0 = 3.5$ K/day. To examine the sensitivity to forcing amplitude, we also perform experiments with $Q_0 = 2.5, 3.0, 4.0, 4.5$ K/day. The warming at 945 hPa over the Arctic region (67.5° – $90^\circ N$) in ALL runs is found to vary between 8.2 and 12.8 K as the imposed heating amplitudes vary between $Q_0 = 2.5$ and 4.5 K/day. Such ATA values are comparable to the projected annual mean AA that is likely to exceed $8.3^\circ C$ during 2080–2099 in the representative concentration pathway 8.5 (RCP8.5) scenario with respect to the historical scenario during 1980–1999 as reported in the Intergovernmental Panel on Climate Change (IPCC) Fifth Assessment (AR5) report (Collins et al., 2013). Forcing amplitudes smaller than 2.5 K/day cause insignificant responses in the stratosphere and thus are not presented.

To aid the interpretation of the underlying dynamical mechanisms, especially the contributions from the stratosphere-troposphere coupling dynamics, we perform another set of experiments, using the no-vortex configuration of our simple model. The no-vortex experiments are employed to remove the stratosphere-troposphere coupling and thus to isolate the tropospheric dynamics alone. We integrate the model for 18,000 days (equivalent to 50 years under perpetual winter conditions) in both standard and no-vortex runs.

3. Results

3.1. The Zonal Mean Zonal Wind Response to Regional ATA

First, we present the zonal mean zonal wind response in the idealized AGCM experiments with imposed heating over ESC, BDL, and BKS regions, separately, in Figures 2a–2c. In response to ESC heating, the simulated atmospheric circulation shows an equatorward shift of the NH midlatitude tropospheric jet characterized by a strengthening on the equatorward flank of the climatological jet and a weakening on the poleward flank (Figure 2a). The stratospheric polar vortex shows a strengthening above 50 hPa while a weakening below that. This response is qualitatively similar to the regression results in observations (Figure S3a: except that the observations show a stronger and more equatorward located jet increase in the stratosphere) and the modeling results in McKenna et al. (2018). Analysis of the Eliassen-Palm (EP) flux (Figure S4a) shows that the strengthening of the stratospheric polar vortex poleward of $60^\circ N$ is primarily associated with a downward wave propagation anomaly, which is due to a destructive interference in Zonal Wave 1 (not shown). The weakening of the stratospheric zonal mean zonal wind over the midlatitudes is due to the convergence of EP flux anomaly, dominated by its meridional component (not shown).

The circulation response in the other two runs, with prescribed heating over BDL (Figure 2b) and BKS (Figure 2c), also shows an equatorward shift of the NH midlatitude tropospheric jet but, unlike Figure 2a, we here see a weakening of the stratospheric polar vortex. Comparing the two runs, the weakening of the stratospheric polar vortex is slightly stronger in the BKS run than the BDL run. These patterns also qualitatively resemble the observed results in the regression analysis except in the low-latitude stratosphere for the BDL case (Figure S3bc). We find that the enhanced EP flux convergence, dominated by the meridional component over the midlatitudes (not shown) and vertical component over the high-latitudes (Figure S4b), is

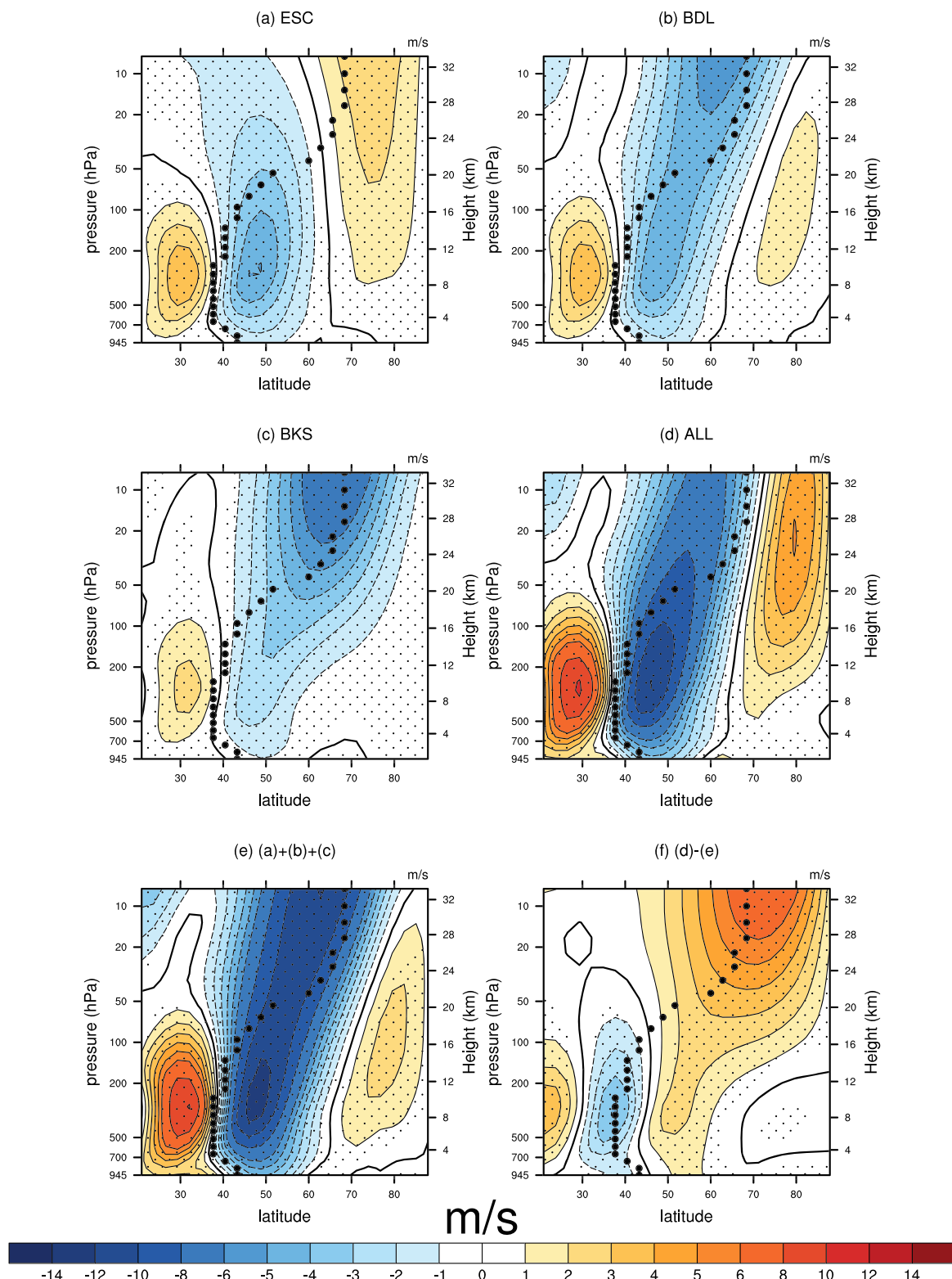


Figure 2. Response of zonal mean zonal wind (color shadings and contours, with contour interval of 1 m/s up to $-/+6$ and 2 m/s beyond that) with a heating amplitude of $Q_0 = 3.5 \text{ K/day}$ in (a) ESC, (b) BDL, (c) BKS, and (d) ALL experiments. (e) The sum of the circulation responses to individual regional forcings and (f) the difference between (d) and (e). Black dots represent the climatological location of jet maximum. Stippling denotes the regions where the response is statistically significant at the 95% confidence level using a two-sided *t* test.

responsible for the weaker stratospheric polar vortex due to BDL warming. The widespread weakening of the stratospheric polar vortex associated with BKS warming is primarily due to the enhanced upward wave propagation (Figure S4c), as reported in Zhang et al. (2017) and McKenna et al. (2018). Additional decomposition of Zonal Wave 1 shows a constructive linear interference for BKS and partially constructive linear interference for BDL (not shown).

The perturbation experiment ALL, with imposed heating over all three regions simultaneously, shows a stronger equatorward shift of the tropospheric jet and a dipole structure in the stratospheric polar vortex with a strengthening poleward of 70° N and a weakening over the midlatitudes (Figure 2d). Interestingly, the linear addition of the zonal mean zonal wind response to regional ATA (Figure 2e), as obtained from the first three standard runs, is not identical to the response obtained from ALL (Figure 2d). In particular, the sum of the responses to regional ATA actually overestimates the response to simultaneous forcing in most regions in the midlatitudes. As a result, the difference between Figures 2d and 2e, as shown in Figure 2f, resembles a positive Northern Annular Mode (NAM)-like structure with a stronger polar vortex in the stratosphere, a poleward shift of the midlatitude jet in the troposphere, and a weakening of the tropospheric jet at the jet core. The pattern is robust over a range of imposed forcing amplitudes (to be discussed later). Additionally, we find that the circulation response to regional ATA is also not linearly additive when any two regions of Arctic temperature anomalies are specified (not shown).

3.2. Non-Additivity and Stratosphere-Troposphere Coupling

Here we explore the non-additivity of the responses and the underlying dynamical mechanism. The vertically coherent structure in the non-additivity component, as shown in Figure 2f, suggests a possible role of the stratosphere-troposphere coupling. To examine the contribution of stratosphere-troposphere coupling, we make use of the additional experiments with the no-vortex configuration of the model.

First, we quantify the percentage of non-additivity by calculating the absolute value of the ratio between the non-additivity component and response to ALL. Figure 3a shows the percentage ratio between Figures 2d and 2f, and the non-additivity of about 10–60% can be seen in the midlatitude troposphere and stratosphere and is considerable to the total response. We focus on 40°–60°N where the maximum zonal mean zonal wind anomaly is found in Figure 2d. In order to assess the stratospheric influence, we examine the corresponding results in the no-vortex runs. Since no-vortex configuration has no climatological stratospheric polar vortex and thus no stratosphere-troposphere coupling, only the tropospheric dynamics is operative. Figure S5 is similar to Figure 2 but in the no-vortex configuration. When comparing the percentage of non-additivity between the standard and no-vortex configuration (Figures 3a and 3b), the amount of non-additivity in the troposphere is significantly reduced between 40° and 60°N in the latter. This confirms a downward influence of stratosphere-troposphere coupling in amplifying the non-additivity in the troposphere. However, since non-additivity is still present in the no-vortex configuration, tropospheric dynamics likely also play a role in causing the non-additivity.

We note that the no-vortex configuration does not exactly represent the tropospheric component of the standard run because of the difference in their climatological states. Additional nudging experiments (Text S1) are performed to examine the robustness of our conclusions by isolating the contribution of the tropospheric dynamics (TP) versus the stratosphere-troposphere coupling (SP) to the non-additivity. Figures S6a and S6b are similar to Figure 2f but by using the TP runs and SP runs, respectively. It can be seen that in the middle-to-lower troposphere, the contribution from tropospheric dynamics is smaller than the total non-additivity (contrast Figures S6a and 2f) and the contribution from stratosphere-troposphere coupling is significant (Figure S6b). However, we also note that the sum of TP and SP does not fully recover the total non-additivity response (not shown), making the quantitative attribution of non-additivity to TP and SP challenging.

3.3. Variation of Non-Additivity With Forcing Amplitude

Next, we quantify how non-additivity varies with forcing amplitude. As discussed above, Figure 3a shows the percentage of non-additivity at $Q_0 = 3.5$ K/day. Qualitatively similar patterns are found over a range of forcing amplitudes, and the percentage ratio generally tends to increase with forcing amplitude in both the troposphere and stratosphere (Figures S7a, S7c, S7e, and S7g). To summarize the results, we plot the relation between the forcing amplitude and the non-additivity at two grid points: one at 700 hPa, 50°N to

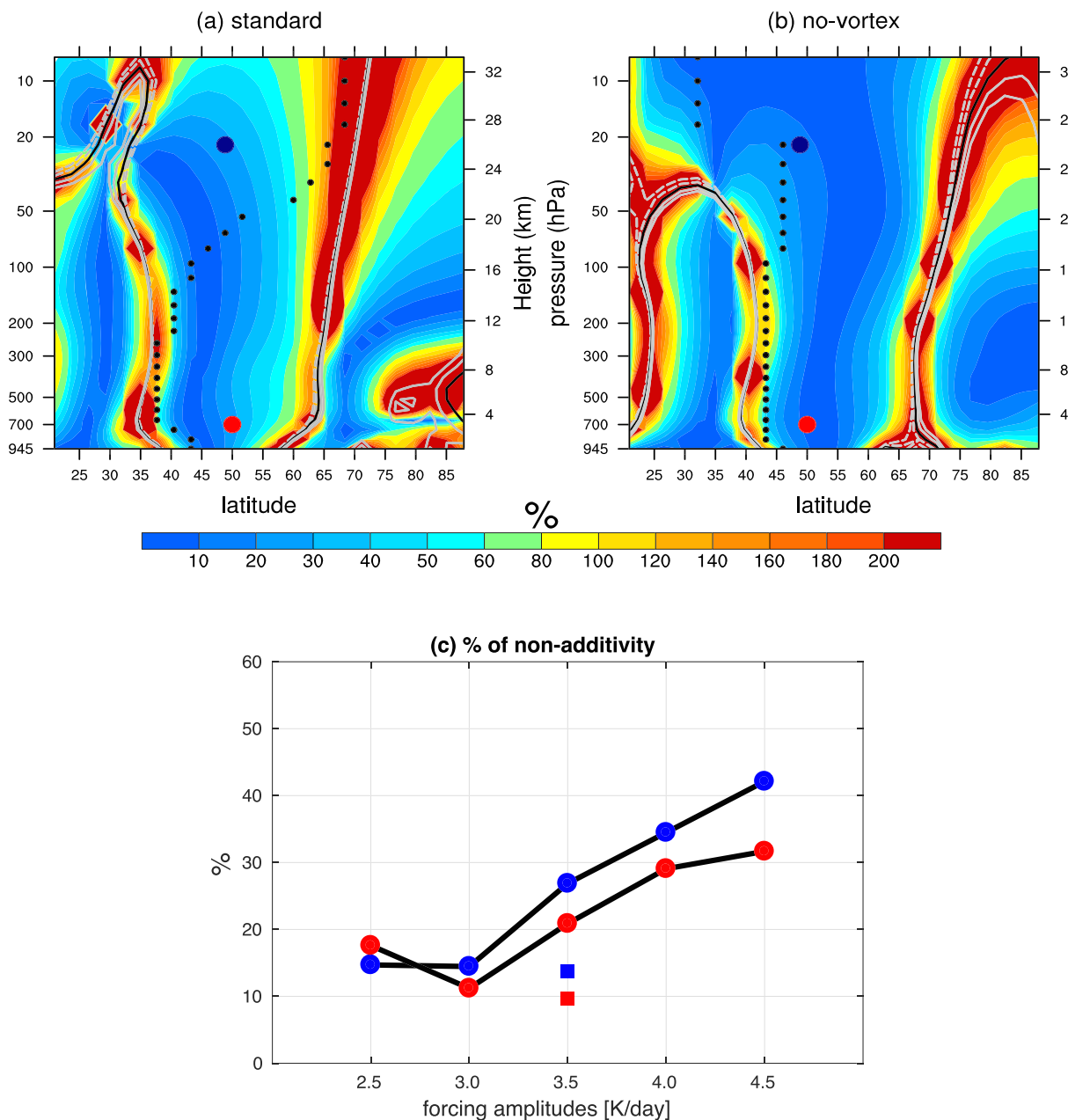


Figure 3. (a) Absolute value of percentage of non-additivity in zonal mean zonal wind response as obtained with 3.5 K/day forcing amplitude. The ratio percentage is calculated as residual (Figure 2f) divided by ALL (Figure 2d). The values in the denominator (ALL) that lie between -0.2 and $+0.2$ m/s are shown in gray contours with contour interval of 0.1 m/s, where negative values are shown in dashed lines, positive values are shown in solid lines, and zero value is shown in black. Black dots represent the climatological location of the jet maxima. (b) Similar to (a) except for the no-vortex runs. (c) Relation between the forcing amplitude and non-additivity ratio at 700 hPa, 50°N (red dots, also in a and b) and 20 hPa, 50°N (blue dots, also in a and b in dark blue dot), respectively, in standard configuration. The corresponding values using no-vortex configuration are shown in squares.

represent the midlatitude troposphere and the other at 20 hPa, 50°N to represent the midlatitude stratosphere, respectively (see red and dark blue dots in Figure 3a). We choose 50°N because it approximately collocates with the maximum jet anomaly over the midlatitudes (Figure 2d). We find that the percentage of non-additivity in the troposphere first decreases from 2.5 to 3.0 K/day heating rate and then increases steadily from about 11% to 32% when heating rate increases from 3.0 to 4.5 K/day. In the stratosphere the non-additivity is approximately the same with heating rates of 2.5 and 3.0 K/day and increases significantly from about 14% to 42% with increasing heating rate. As a comparison, the

no-vortex results are also shown (see squares), but the non-additivity ratio reduces by about 50% than the counterparts in the standard model configuration with 3.5 K/day heating rate. We find that the percentage of non-additivity in the midlatitude middle-to-lower troposphere is consistently lower in no-vortex runs compared to standard runs over a range of forcing amplitudes except 3 K/day (Figures S7 and S8).

4. Conclusions and Discussion

In this study, we have explored the linear additivity of the midlatitude circulation response to regional Arctic heating, the underlying dynamical mechanism, and its dependence on forcing amplitude using a simplified AGCM. Specifically, we have found the following:

- Regional Arctic heating has similar impacts on the tropospheric zonal mean zonal wind with an equatorward shift of the midlatitude tropospheric jet. But differences in the response are seen in the stratosphere. While the stratospheric polar vortex generally weakens with imposed heating over the BKS and BDL regions, the stratospheric polar vortex strengthens above 50 hPa when the forcing is imposed over the ESC region.
- The zonal mean zonal wind responses to regional Arctic heating are not linearly additive, and the sum of the responses to regional heating overestimates the response to simultaneous forcing in most midlatitude regions. As a result, a positive NAM-like vertically coherent response is found in the residual term.
- Stratosphere-troposphere coupling plays an important role in amplifying the non-additivity in the tropospheric response. Specifically, non-additivity of the stratospheric response and its downward influence on the troposphere is the key.
- For a warming of about 10 K over the Arctic (corresponding to imposed heating rate of 3.5 K/day), non-additivity could contribute about 10–60% to the total response in the midlatitude troposphere and stratosphere and is not negligible. In addition, the non-additivity also generally increases with forcing amplitude.

We would like to emphasize, as mentioned in section 1, that considerable diversities exist among model responses to Arctic sea ice loss, part of which can be attributable to different spatial patterns of the forcing (Screen et al., 2018, and references therein). As found in this study, responses to sea ice loss over different regions can interact nonlinearly to affect the midlatitude circulation response. The results suggest that, because of this non-additivity, studying the response to regional sea ice loss might not provide the correct picture of the consequences of pan-Arctic sea ice loss in decadal time scale. And pan-Arctic sea ice forcing, rather than regional sea ice forcing, should be used for studies whose focus is the impact of decadal sea ice melting.

In addition, we find that stratosphere-troposphere coupling plays a critical role in understanding not only response to individual regional Arctic heating but also the non-additivity of the tropospheric circulation response to regional heating. In particular, the non-additivity is amplified by active stratosphere-troposphere coupling through downward influence. It is therefore important to fully and correctly represent the stratospheric circulation in order to simulate an accurate response to sea ice loss in model experiments. We note here that tropospheric dynamics likely also contribute to the non-additivity and will leave it for future work.

In summary, the results presented here using idealized AGCM experiments confirm the results of Screen (2017) using a comprehensive AGCM. In both Screen (2017) and our study, considerable non-additivity in the circulation response is found: In particular, the sum of responses to regional forcing is found to overestimate the response to simultaneous forcing. Building on the findings of Screen (2017), we further examine the role of stratosphere-troposphere coupling and sensitivity to forcing amplitude. We note that the model used by Screen (2017) does not have a well-resolved stratosphere (“low-top”), so the non-additivity found in Screen (2017) could possibly be underestimated. Therefore, it will be worth revisiting that study but with a stratosphere-resolving comprehensive AGCM (“high-top”) and reassessing the contribution of non-additivity to the large-scale atmospheric circulation and regional extremes. For the mechanism underlying the non-additivity, it is possible that regional circulation response is more prone to develop with regionally confined forcing than extended forcing and therefore causes an overestimation of the circulation response. But more work is needed to better understand it.

Data Availability Statement

Data will be available at the Columbia Academic Commons website (<https://academiccommons.columbia.edu/doi/10.7916/d8-01bs-g908>).

Acknowledgments

We would like to thank Drs. Edwin Gerber, Paul Kushner, Karen L. Smith, Pengfei Zhang, and Mingfang Ting for useful discussion and suggestions at different stages of this work. We thank anonymous reviewers for their comments and suggestions. We would like to acknowledge the support from Dr. Wen-wen Tung and the supercomputing resources at Purdue University to conduct this work. B. De and Y. Wu are supported by the NSF (AGS-1406962). B. De also acknowledge the support from Bilsland Dissertation Fellowship, awarded by Purdue University. L. M. P. is grateful to the U.S. National Science Foundation for its generous support (OPP-1603350). Y. W. also acknowledges the support from the Lamont Center for Climate and Life Fellowship.

References

- Barnes, E. A., & Screen, J. A. (2015). The impact of arctic warming on the midlatitude jet-stream: Can it? Has it? Will it? *Wiley Interdisciplinary Reviews Climate Change*, 6, 277–286. <https://doi.org/10.1002/wcc.337>
- Cavalieri, D. J., Parkinson, C. L., Gloersen, P., & Zwally, H. J. (1996). *Sea ice concentrations from Nimbus-7 SMMR and DMSP SSM/I-SSMIS passive microwave data, Version 1*. NASA National Snow and Ice Data Center Distributed Active Archive Center. <https://doi.org/10.5067/8GQ8LZQVLOVL>
- Chen, X., & Luo, D. (2017). Arctic sea ice decline and continental cold anomalies: Upstream and downstream effects of Greenland blocking. *Geophysical Research Letters*, 44, 3411–3419. <https://doi.org/10.1002/2016GL072387>
- Cohen, J., Screen, J. A., Furtado, J. C., Barlow, M., Whittleston, D., Coumou, D., et al. (2014). Recent Arctic amplification and extreme mid-latitude weather. *Nature Geoscience*, 7, 627–637. <https://doi.org/10.1038/ngeo2234>
- Collins, M., Knutti, R., Arblaster, J., Dufresne, J.-L., Fichefet, T., Friedlingstein, P., et al. (2013). Long-term climate change: Projections, commitments and irreversibility. In T. F. Stocker, D. Qin, G.-K. Plattner, M. Tignor, S. K. Allen, J. Doschung, et al. (Eds.), *Climate change 2013: The physical science basis. Contribution of Working Group I to the Fifth Assessment Report of the Intergovernmental Panel on Climate Change* (pp. 1029–1136). Cambridge, UK: Cambridge University Press. <https://doi.org/10.1017/CBO9781107415324.024>
- De, B., & Wu, Y. (2018). Robustness of the stratospheric pathway in linking the Barents-Kara Sea sea ice variability to the mid-latitude circulation in CMIP5 models. *Climate Dynamics*, 53, 193–207. <https://doi.org/10.1007/s00382-018-4576-6>
- Dee, D. P., & Coauthors (2011). The ERA-Interim reanalysis: Configuration and performance of the data assimilation system. *Quarterly Journal of the Royal Meteorological Society*, 137, 553–597. <https://doi.org/10.1002/qj.828>
- Held, I. M., & Suarez, M. J. (1994). A proposal for the intercomparison of the dynamical cores of atmospheric general circulation models. *Bulletin of the American Meteorological Society*, 75, 1825–1830. [https://doi.org/10.1175/1520-0477\(1994\)075<1825:APFTIO>2.0.CO;2](https://doi.org/10.1175/1520-0477(1994)075<1825:APFTIO>2.0.CO;2)
- Kim, B.-M., Son, S.-W., Min, S.-K., Jeong, J.-H., Kim, S.-J., Zhang, X., et al. (2014). Weakening of the stratospheric polar vortex by Arctic sea-ice loss. *Nature Communications*, 5, 4646. <https://doi.org/10.1038/ncomms5646>
- Kug, J. S., Jeong, J. H., Jang, Y. S., Kim, B. M., Folland, C. K., Min, S. K., & Son, S. W. (2015). Two distinct influences of Arctic warming on cold winters over North America and East Asia. *Nature Geoscience*, 8, 759–762. <https://doi.org/10.1038/ngeo2517>
- McCusker, K. E., Fyfe, J. C., & M, M. S. (2016). Twenty-five winters of unexpected Eurasian cooling unlikely due to Arctic sea-ice loss. *Nature Geoscience*, 9, 838–842. <https://doi.org/10.1038/ngeo2820>
- McKenna, C. M., Bracegirdle, T. J., Shuckburgh, E. F., Haynes, P. H., & Joshi, M. M. (2018). Arctic sea ice loss in different regions leads to contrasting Northern Hemisphere impacts. *Geophysical Research Letters*, 45, 945–954. <https://doi.org/10.1002/2017GL076433>
- Mori, M., Watanabe, M., Shiogama, H., Inoue, J., & Kimoto, M. (2014). Robust Arctic sea-ice influence on the frequent Eurasian cold winters in past decades. *Nature Geoscience*, 7, 869–873. <https://doi.org/10.1038/ngeo2277>
- Ogawa, F., Keenlyside, N., Gao, Y., Koenigk, T., Yang, S., Suo, L., et al. (2018). Evaluating impacts of recent arctic sea ice loss on the Northern Hemisphere winter climate change. *Geophysical Research Letters*, 45, 3255–3263. <https://doi.org/10.1002/2017GL076502>
- Overland, J. E., & Wang, M. (2018). Arctic-midlatitude weather linkages in North America. *Polar Science*, 16, 1–9. <https://doi.org/10.1016/j.polar.2018.02.001>
- Polvani, L. M., & Kushner, P. J. (2002). Tropospheric response to stratospheric perturbations in a relatively simple general circulation model. *Geophysical Research Letters*, 29(7), 18–1–18–4. <https://doi.org/10.1029/2001GL014284>
- Screen, J. A. (2017). Simulated atmospheric response to regional and pan-Arctic sea ice loss. *Journal of Climate*, 30, 3945–3962. <https://doi.org/10.1175/JCLI-D-16-0197.1>
- Screen, J. A., Deser, C., Smith, D., Zhang, X., Blackport, R., Kushner, P. J., et al. (2018). Consistency and discrepancy in the atmospheric response to Arctic sea-ice loss across climate models. *Nature Geoscience*, 11, 155–163. <https://doi.org/10.1038/s41561-018-0059-y>
- Screen, J. A., Deser, C., & Sun, L. (2015). Projected changes in regional climate extremes arising from Arctic sea ice loss. *Environmental Research Letters*, 10, 084006.
- Screen, J. A., & Simmonds, I. (2010). The central role of diminishing sea ice in recent arctic temperature amplification. *Nature*, 464, 1334–1337. <https://doi.org/10.1038/nature09051>
- Shepherd, T. G. (2016). Effects of a warming arctic. *Science*, 353, 989–990. <https://doi.org/10.1126/science.aag2349>
- Smith, K. L., Fletcher, C. G., & Kushner, P. J. (2010). The role of linear interference in the annular mode response to extratropical surface forcing. *Journal of Climate*, 23, 6036–6050. <https://doi.org/10.1175/2010JCLI3606.1>
- Sun, L., Deser, C., & Tomas, R. A. (2015). Mechanisms of stratospheric and tropospheric circulation response to projected Arctic sea ice loss. *Journal of Climate*, 28, 7824–7845. <https://doi.org/10.1175/JCLI-D-15-0169.1>
- Sun, L., Perlitz, J., & Hoerling, M. (2016). What caused the recent “warm arctic, cold continents” trend pattern in winter temperatures? *Geophysical Research Letters*, 43, 5345–5352. <https://doi.org/10.1002/2016GL069024>
- Wu, Y., & Smith, K. L. (2016). Response of Northern Hemisphere midlatitude circulation to Arctic amplification in a simple atmospheric general circulation model. *Journal of Climate*, 29, 2041–2058. <https://doi.org/10.1175/JCLI-D-15-0602.1>
- Zhang, P., Wu, Y., Simpson, I. R., Smith, K. L., Zhang, X., De, B., & Callaghan, P. (2018). A stratospheric pathway linking a colder Siberia to Barents-Kara Sea sea ice loss. *Science Advances*, 4, eaat6025. <https://doi.org/10.1126/sciadv.aat6025>
- Zhang, P., Wu, Y., & Smith, K. L. (2017). Barents Kara Sea Sea Ice variability to the midlatitude circulation in a simplified model. *Climate Dynamics*, 50, 527–539. <https://doi.org/10.1007/s00382-017-3624-y>